JOURNAL OF GUIDANCE, CONTROL, AND DYNAMICS
Vol. 31, No. 6, November–December 2008

Rapid Optimal Multiburn Ascent Planning and Guidance

Ping Lu* and Brian J. Griffin†
Iowa State University, Ames, Iowa 50011-2271
Gregory A. Dukeman‡
NASA Marshall Space Flight Center, Huntsville, Alabama 35812
and
Frank R. Chavez§
U.S. Air Force Research Laboratory, Kirtland Air Force Base, New Mexico 87117

DOI: 10.2514/1.36084

This paper provides detailed development of an analytical multiple-shooting method for rapid and reliable generation of the optimal exoatmospheric ascent trajectory of a launch vehicle. The trajectory consists of two burns (stages) and an optimal coast arc between the two burns. The problem is known to be highly sensitive and challenging. The problem solution is given in closed form and quadratures and key development details are presented. An in-depth analysis of a transversality condition in the optimal ascent problem is conducted to gain better understanding of the problem. The analysis reveals several properties that allow us to overcome a numerical difficulty caused by a scaling mismatch in the transversality condition. This measure is instrumental in increasing the convergence reliability of the algorithm. A dogleg trust-region method that is more robust than the classical Newton–Raphson method is employed for the numerical solution. The multiple-shooting formulation, constraint simplification, and more sophisticated numerical method are all aimed at enhancing the robustness of the algorithm for this otherwise difficult problem. The final product of combining all of these techniques is a very reliable, effective, and fast algorithm. Such an algorithm can be a valuable tool in rapid planning of launch missions and in onboard applications for closed-loop guidance.

I. Introduction

LAUNCH ascent mission planning and guidance is an engineering area in which routine applications of optimization tools and optimal control theory are a necessity rather than a nicety. Indeed, onboard algorithms for solving the optimal ascent problem have been the foundation of closed-loop ascent guidance for upper stages of launch vehicles since the 1960s. The examples of classical exoatmospheric optimal ascent guidance algorithms include the iterative guidance mode employed for the Saturn V rockets [1] and the powered explicit guidance for the space shuttle [2]. When the optimal ascent problem is solved online repeatedly with the current condition as the initial condition, the guidance solution is, in effect, a closed loop.

For multiple-stage launch vehicles or even within the same stage, it is well known that allowing a coast arc of optimal duration between two burns can reduce propellant consumption (or increase orbital-insertion mass), in some cases, very appreciably. In other scenarios, a long coast is necessary between two burns, such as insertion into high-altitude orbits or orbital transfers. However, there are additional challenges resulting from the presence of coast arcs and multiple burns. Multiple burns and coast arcs typically render the optimal control problem much more sensitive and increase the difficulty of achieving convergence of the algorithm. This heightened sensitivity is largely due to two reasons:

1) Long coast arcs tend to amplify any variations in the condition at the beginning of the coast.

2) The final stage/burn usually has a much smaller thrust acceleration, and it would be incapable of making large flight-path corrections (indeed, the last burn in many orbital-insertion cases is almost tangential, mainly responsible for pushing the velocity to the required value).

The fact that even today, missions with multiple burns and coast arcs are planned and executed by ground control is probably attributable in no small part to these challenges. The recent ongoing efforts at striving to achieve the capabilities of responsive space launch mission planning and operations and autonomous space operations have brought renewed strong interest in this subject.

To overcome the aforementioned difficulties, researchers have continued to seek more robust and reliable methods to handle the optimal ascent problem with multiple burns and coast arcs. References [3–9] represent only a small sampling of the literature. With the exception of the work by Dukeman and Calise [8] and Dukeman [9], most existing work treats the problem essentially in a single-shooting formulation; that is, the missing initial costate is iterated on to satisfy the terminal constraints and transversality conditions. References [8,9] employ a numerical multiple-shooting approach to the problem, including the endoatmospheric ascent portion.

In this paper, we present an analytical multiple-shooting method for exoatmospheric multiburn optimal ascent. Work in this direction is first initiated in [10]. This paper completes the effort and reports the key elements of the algorithm. The overarching theme in this effort is to strive for enhanced robustness and reliability of the algorithm. In this approach, the optimal trajectory is treated in segments of burn and coast arcs. The costate in each segment is expressed in closed-form solution and the state is expressed in an analytical solution involving thrust quadratures. Such a multiple-shooting formulation reduces the sensitivity of the problem with respect to the parameters to be found, especially beneficial to the cases with long coast arcs. The orbital-insertion conditions, transversality conditions, and

Presented as Paper 6773 at the AIAA Guidance, Navigation, and Control Conference, Hilton Head, SC, 20–23 August 2007; received 6 December 2007; revision received 30 May 2008; accepted for publication 10 June 2008.

*Professor, Department of Aerospace Engineering, 2271 Howe Hall; plu@iastate.edu, Associate Fellow AIAA.

†Graduate Research Assistant, Aerospace Engineering, 2271 Howe Hall; currently Aerospace Engineer, NASA Dryden Flight Research Center; Brian.J.Griffin@nasa.gov.

‡Guidance and Navigation Specialist, Mail Stop EV42; Greg.Dukeman@nasa.gov.

§Research Aerospace Engineer, Space Vehicles Directorate. Senior Member AIAA.

matching continuity conditions at the break points constitute a system of nonlinear algebraic equations with an analytical Jacobian. For numerical solutions, the existing work almost invariably uses the classical or some modified version of the Newton–Raphson method. Here, we adopt the highly regarded Powell's dogleg method [11] for improved robustness and reliability of the overall algorithm in more difficult, and even possibly singular, cases (in which the optimal coast time reduces to zero).

Another major component of this paper is the detailed analysis of certain aspects of the class of optimal ascent problems under discussion. An analysis helps correct a potential misconception that the Hamiltonian is *always zero everywhere* along the optimal trajectory in a free-final-time multiburn problem. The correct answer depends on whether there are burn or coast arcs in which the flight times are prescribed. The analysis of a transversality condition reveals several interesting properties that are previously unknown to the community, to the best of our knowledge. The results afford us a number of easy ways to satisfactorily resolve a numerical scaling mismatch issue in the transversality condition that could otherwise severely hinder convergence reliability of the algorithm. All of these measures contribute to a robust and fast algorithm for optimal multiburn ascent planning and closed-loop guidance. The algorithm is verified with an industry-standard software package, Optimal Trajectories by Implicit Simulation (OTIS) [12].

II. Multistage Optimal Ascent Problem with Coast

Instead of seeking maximum generality, we choose to tacitly present the development in a burn-coast-burn pattern for readability of the presentation. There is no methodological difficulty to extend the development here to any combinations of other prescribed numbers of burn and coast arcs. Borrowing the shuttle terminology, we will refer to the burnout of the first vacuum burn/stage as the main engine cutoff (MECO). Staging, if any, occurs at the end of the burnout of the first stage. A coast arc is allowed right after staging (but the optimal coast time can turn out to be zero). The second burn after the coast is called the orbital maneuver system (OMS) burn. For on-orbit maneuvers, it is understood that both burns can be made by the same engine, and there is no staging at the end of the first burn.

A. Problem Formulation

After the launch vehicle clears the dense atmosphere, the three-dimensional point-mass equations of motion in vacuum are

$$\dot{\boldsymbol{r}} = \boldsymbol{V} \tag{1}$$

$$\dot{\boldsymbol{V}} = \mathbf{g}(\boldsymbol{r}) + \frac{T\mathbf{1}_T}{m(t)} \tag{2}$$

$$\dot{m} = -\frac{T}{g_0 I_{\text{sp}}} \tag{3}$$

where $\boldsymbol{r} \in R^3$ and $\boldsymbol{V} \in R^3$ are the position and inertial velocity vector in an inertial frame. The gravitational acceleration $\boldsymbol{g}$ is a function of $\boldsymbol{r}$, and g_0 is the magnitude of $\boldsymbol{g}$ at a reference radius R_0. The engine thrust magnitude is T, and the unit vector $\mathbf{1}_T$ defines the direction of the thrust vector. The vehicle mass rate $\dot{m}$ is determined by the last preceding equation, in which I_{sp} is the specific impulse of the engine. An ingenious approximation to the gravitational acceleration is the so-called linear gravity approximation [13]:

$$\boldsymbol{g} = -\frac{\mu\,\boldsymbol{r}}{\bar{r}^2\,\bar{r}} = -\bar{\omega}^2\boldsymbol{r} \tag{4}$$

where μ is the gravitational parameter of the Earth, $\bar{r}$ is another reference radius (e.g., an average value of r along the ascent trajectory), and $\bar{\omega} = \sqrt{\mu/\bar{r}^3}$ is the Schuler frequency at $\bar{r}$. This approximation preserves the more important characteristic of the gravity in ascent flight, the direction, and enables one to obtain an analytical solution to the costate equation in optimal exoatmospheric flight, as shall be seen later. The minor gravity magnitude difference caused by this approximation in ascent typically has little influence on the validity of the solution. For a multiple-burn trajectory, a different value of the $\bar{\omega}$ may be used for each burn arc so that any approximation effect on gravity magnitude is reduced.

An assumption on the class of problems treated is that the initial condition $(\boldsymbol{r}_0, \boldsymbol{V}_0)$ is known. Another practical assumption on the methodology developed in this paper is that the burn times of all the powered stages except for the last are all determined by their propellant loading and mass flow rate. The burn time of the last powered stage and the coast times are optimized. Therefore, the final time for the complete trajectory is free. For two-burn orbital transfers, the burn time of the first burn may also need to be optimized. In such a case, all the developments and equations in the rest of this paper remain valid, and one additional interior switching condition will be added (cf. [8]).

For better numerical conditioning, the distances are normalized by R_0, the velocities by $\sqrt{R_0 g_0}$, and the time by $\sqrt{R_0/g_0}$. With some abuse of notation, we will still use $\boldsymbol{r}$ and $\boldsymbol{V}$ to denote the dimensionless position and velocity vector, respectively. With the preceding linear gravity approximation, the dimensionless equations of motion are

$$\boldsymbol{r}' = \boldsymbol{V} \tag{5}$$

$$\boldsymbol{V}' = -\omega^2\boldsymbol{r} + A_T\mathbf{1}_T \tag{6}$$

where the differentiation is with respect to the nondimensional time $\tau = t/\sqrt{R_0/g_0}$, $\omega = \sqrt{(R_0/\bar{r})^3}$ is the nondimensional Schuler frequency, and $A_T = T/mg_0$ is the instantaneous thrust acceleration in g. The mass rate equation becomes

$$m' = -\frac{T}{c} \tag{7}$$

where $c = I_{\text{sp}}/\sqrt{R_0/g_0^3}$ is a (possibly different) constant for each powered stage. Note that the mass need not be normalized, as it only appears in the equations of motion in the dimensionless quantity $A_T = T/mg_0$. The orbital-insertion conditions are generally in terms of k equality constraints ($k \le 6$) on the final state:

$$\boldsymbol{\phi}\,(\boldsymbol{r}_f, \boldsymbol{V}_f) = 0 \tag{8}$$

The optimal thrust direction vector $\mathbf{1}_T$ is determined by the solution of the optimal control problem that minimizes the performance index:

$$J = -\int_{\tau_0}^{\tau_f} m'\,\mathrm{d}\tau = \int_{\tau_0}^{\tau_f} \frac{T}{c}\,\mathrm{d}\tau \tag{9}$$

It is clear that this performance index amounts to minimization of propellant consumption for a given initial mass. The standard optimal control theory [14] calls for the use of the Hamiltonian:

$$\begin{aligned} H &= \boldsymbol{p}_r^T\boldsymbol{V} - \omega^2\boldsymbol{p}_V^T\boldsymbol{r} + \boldsymbol{p}_V^T\mathbf{1}_T A_T - p_m\frac{T}{c} - \frac{T}{c} \\ &= \boldsymbol{p}_r^T\boldsymbol{V} - \omega^2\boldsymbol{p}_V^T\boldsymbol{r} + T\left(\frac{\boldsymbol{p}_V^T\mathbf{1}_T}{mg_0} - \frac{p_m}{c} - \frac{1}{c}\right) := H_0 + TS \end{aligned} \tag{10}$$

In the preceding Hamiltonian, $\boldsymbol{p}_r$ and $\boldsymbol{p}_V$ constitute the costate vector, satisfying the differential equation:

$$\begin{pmatrix} \boldsymbol{p}_r' \\ \boldsymbol{p}_V' \end{pmatrix} = -\begin{pmatrix} \partial H/\partial \boldsymbol{r} \\ \partial H/\partial \boldsymbol{V} \end{pmatrix} = \begin{pmatrix} \omega^2\boldsymbol{p}_V \\ -\boldsymbol{p}_r \end{pmatrix} \tag{11}$$

In particular, $\boldsymbol{p}_V$ is called the primer vector because the optimal thrust direction $\mathbf{1}_T = \boldsymbol{p}_V/\|\boldsymbol{p}_V\|$ [15]. The switching function S determines when to use full thrust and when to coast ($T = 0$). Specifically,

$$T = \begin{cases} T_{\max} & \text{if } S > 0 \\ 0 & \text{if } S < 0 \end{cases} \tag{12}$$

The case of singular thrust arcs (when $S \equiv 0$ in a finite period of time and the thrust takes some intermediate values $0 < T < T_{\max}$) is not considered because it is well known that, except for a few pathological cases, the singular solutions are not optimal in exoatmospheric flight.[16] Suppose in our discussion that the coast of the second stage ends at a to-be-determined time τ_{OMS}. It is then necessary that $S(\tau_{\text{OMS}}) = 0$ [and $S(\tau) > 0$ for $\tau \in (\tau_{\text{OMS}}, \tau_f)$]. Because the total final time τ_f is free for this optimal ascent problem, the Hamiltonian H defined in Eq. (10) is equal to zero in $(\tau_{\text{MECO}}, \tau_f]$ along the optimal trajectory (see Sec. IV.A for more discussion). As a result, the condition $S(\tau_{\text{OMS}}) = 0$ is equivalent to

$$H_0(\tau_{\text{OMS}}) = 0 \tag{13}$$

This equation avoids the computation of the mass costate p_m and thus is preferred to the condition $S(\tau_{\text{OMS}}) = 0$. In light of this observation and other necessary conditions already discussed, we conclude that the mass costate p_m need not be explicitly computed in our problem.

B. Analytical Solution for Burn Arcs

The analytical solutions to the costate equation (11) and analytical solution to state equations (5) and (6), first presented in [13] and later also applied in [17,18], are given next for completeness. Suppose that the starting time for the ascent trajectory is τ_0. Let $\boldsymbol{p}_{V_0}$ and $\boldsymbol{p}_{r_0}$ be the (to-be-determined) initial conditions for the costates at τ_0. Define

$$\boldsymbol{\lambda}(\tau) = \begin{pmatrix} \boldsymbol{p}_V(\tau) \\ -\boldsymbol{p}_r(\tau)/\omega \end{pmatrix}, \qquad \boldsymbol{\lambda}_0 = \begin{pmatrix} \boldsymbol{p}V_0 \\ -\boldsymbol{p}/\omega r_0 \end{pmatrix}$$

For $\tau \geq \tau_0$, the costate equation (11) has a closed-form solution:

$$\boldsymbol{\lambda}(\tau) = \begin{bmatrix} \cos[\omega(\tau-\tau_0)]I_3 & \sin[\omega(\tau-\tau_0)]I_3 \\ -\sin[\omega(\tau-\tau_0)]I_3 & \cos[\omega(\tau-\tau_0)]I_3 \end{bmatrix} \quad \boldsymbol{\lambda}_0 := \Phi(\tau-\tau_0)\boldsymbol{\lambda}_0 \tag{14}$$

where I_3 is a 3×3 identity matrix. Define

$$\boldsymbol{I}_c(\tau, \tau_0) = \int_{\tau_0}^{\tau} \mathbf{1}_{p_V}(\zeta) \cos(\omega\zeta) A_T(\zeta)\, \mathrm{d}\zeta := \int_{\tau_0}^{\tau} \boldsymbol{i}_c(\zeta)\, \mathrm{d}\zeta \in R^3 \tag{15}$$

$$\boldsymbol{I}_s(\tau, \tau_0) = \int_{\tau_0}^{\tau} \mathbf{1}_{p_V}(\zeta) \sin(\omega\zeta) A_T(\zeta)\, \mathrm{d}\zeta := \int_{\tau_0}^{\tau} \boldsymbol{i}_s(\zeta)\, \mathrm{d}\zeta \in R^3 \tag{16}$$

where $\mathbf{1}_{p_V} = \boldsymbol{p}_V / \|\boldsymbol{p}_V\|$. Note that thrust acceleration $A_T(\cdot)$ is time-varying, because the mass is changing. Also pay attention to the meaning of the time arguments in $\Phi(\tau - \tau_0)$, $\boldsymbol{I}_c(\cdot,\cdot)$, and $\boldsymbol{I}_s(\cdot,\cdot)$ because they will be important in multiburn cases. Let

$$\boldsymbol{x}(\tau) = \begin{pmatrix} \boldsymbol{r}(\tau) \\ \boldsymbol{V}(\tau)/\omega \end{pmatrix}, \qquad \boldsymbol{x} = \begin{pmatrix} \boldsymbol{r}_0 \\ \boldsymbol{V}_0/\omega \end{pmatrix}$$

$$\boldsymbol{I}(\tau, \tau_0) = \begin{bmatrix} \boldsymbol{I}_c(\tau, \tau_0) \\ \boldsymbol{I}_s(\tau, \tau_0) \end{bmatrix} 0 \tag{17}$$

It can be easily verified that the state equations (5) and (6) have the following solution [5]:

$$\boldsymbol{x}(\tau) = \Phi(\tau - \tau_0)\boldsymbol{x}_0 + \Gamma(\tau)\boldsymbol{I}(\tau, \tau_0) \tag{18}$$

where

$$\Gamma(\tau) = \frac{1}{\omega} \begin{bmatrix} \sin(\omega\tau)I_3 & -\cos(\omega\tau)I_3 \\ \cos(\omega\tau)I_3 & \sin(\omega\tau)I_3 \end{bmatrix} \tag{19}$$

The thrust integrals $\boldsymbol{I}_c$ and $\boldsymbol{I}_s$ can be evaluated by a quadrature formula. For example, with $\delta = (\tau - \tau_0)/4$, Milne's rule leads to [18]

$$\boldsymbol{I}_j(\tau, \tau_0) = \frac{(\tau - \tau_0)}{90}[7\boldsymbol{i}_j(\tau_0) + 32\boldsymbol{i}_j(\tau_0 + \delta) + 12\boldsymbol{i}_j(\tau_0 + 2\delta) + 32\boldsymbol{i}_j(\tau_0 + 3\delta) + 7\boldsymbol{i}_j(\tau_0 + 4\delta)], \qquad j = c, s \tag{20}$$

The values of the primer vector $\boldsymbol{p}_V$ at $\tau_0 + i\delta$ are needed in evaluating the thrust integrals, and they are given by Eq. (14) as functions of $\boldsymbol{\lambda}_0$. The errors of the quadratures in Eq. (20) are proportional to δ^7. For a 400 s burn, the dimensionless $\delta^7 = 4.525 \times 10^{-7}$. Our experiences show that computation of the preceding quadratures once over each burn arc is sufficiently accurate for powered-flight arcs up to several hundred seconds. Additional segments in the time grid may be used for much longer powered flight if necessary.

C. Solution for Coast Arcs

For coast flight, where $A_T = 0$, Jezewski [5] propagates the state by continuing to use Eq. (18), which has only the initial response term now. We believe that it is more advantageous to use a more accurate solution approach to the Keplerian motion in a coast arc. The f and g series in orbital mechanics [19] are an option. These series are Taylor series expansions of $\boldsymbol{r}$ and $\boldsymbol{V}$ in time, with all the coefficients expressed as functions of $\boldsymbol{r}_0$ and $\boldsymbol{V}_0$. The inverse-square gravity model is used, and the accuracy of the solution is not compromised by the linear gravity approximation, even with relatively large radial distance changes. A possible drawback of using the f and g series is that for a fixed number of terms in the software for the truncated Taylor series, the accuracy deteriorates as the time of coast increases. Yet another choice is to use the well-established method by Goodyear [20] to solve the Kepler initial value problem as done in [9]. This approach gives a complete Keplerian motion solution to the problem within the machine accuracy that includes the state at a specified future time as the function of the current state ($\boldsymbol{r}_0\boldsymbol{V}_0$) and the gradients of the future state with respect to $\boldsymbol{r}_0$ and $\boldsymbol{V}_0$. This is the method we have adopted in this work.

The costate, on the other hand, may continue to be propagated by Eq. (14) during the coast. A second option is to employ the analytical solution to the costate in Keplerian motion developed by Lawden [15]. This approach preserves the model of an inverse-square gravity field, but the solution is given in a rotating frame related to the orbital motion. Once the Kepler initial value problem is solved, the corresponding costate can be readily transformed back to the original inertial frame. In this work, we choose to propagate the costate by Eq. (14) for its simplicity. In any approach, the state and costate at the end of the coast are uniquely defined by their values at the beginning of the coast and the coast time.

D. Multiple-Shooting Formulation

In principle, the optimal exoatmospheric ascent problem from a given initial condition $\{\boldsymbol{r}_0, \boldsymbol{V}_0\}$ with a coast arc is determined by 8 unknowns: $\boldsymbol{p}_{r_0} \in R^3$, $\boldsymbol{p}_{V_0} \in R^3$, τ_{OMS} (the time when coast stops and the second stage burn begins), and the free final time τ_f. The corresponding 8 conditions are the k-terminal conditions in Eq. (8), switching condition Eq. (13), transversality condition $H(\tau_f) = 0$, and the other 6-k transversality conditions (see [17,18] for more detail on how to obtain the remaining 6-k transversality conditions). Directly solving for the 8 unknowns to satisfy the 8 conditions is, in essence, a single-shooting approach. Difficulties in convergence arise when the coast time is just moderately long and/or the thrust acceleration of the last stage is relatively small, because in these cases, the sensitivity of the problem increases and the ability of the final burn to steer the trajectory onto the terminal condition manifold weakens.

To enhance the robustness of convergence of the algorithm, two additional nodes are added to the formulation of the numerical problem. One node is placed at the end of the first powered stage. Let $\tau_{\text{MECO}} > \tau_0$ denote the instant when the engine of the first powered stage shuts down, and recall that τ_{MECO} is considered to be specified. The other node is naturally placed at τ_{OMS} when the coast ends and the second powered stage begins, where τ_{OMS} is to be determined. Figure 1 gives an illustration of this multiple-shooting formulation.

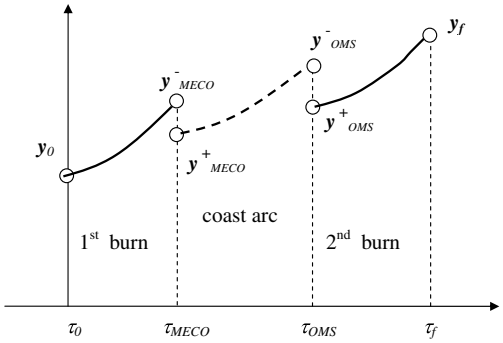

Fig. 1 Multiple-shooting formulation for optimal exoatmospheric ascent with coast.

Define the problem solution vector $\boldsymbol{y} = \text{col}(\boldsymbol{x}\ \boldsymbol{\lambda}) \in R^{12}$. In the interval $(\tau_0, \tau_{\text{MECO}})$, the solution of $\boldsymbol{y}$ is determined by the condition $\boldsymbol{y}_0$ at τ_0 by Eqs. (14) and (18). We will use $\boldsymbol{y}^-_{\text{MECO}}$ to signify the value of $\boldsymbol{y}$ at τ_{MECO} as $\tau \to \tau_{\text{MECO}}$ from the left. Introduce two additional to-be-determined vectors:

$$\boldsymbol{y}^+_{\text{MECO}} = \begin{pmatrix} \boldsymbol{x}^+_{\text{MECO}} \\ \boldsymbol{\lambda}^+_{\text{MECO}} \end{pmatrix}, \qquad \boldsymbol{y}^+_{\text{OMS}} = \begin{pmatrix} \boldsymbol{x}^+_{\text{OMS}} \\ \boldsymbol{\lambda}^+_{\text{OMS}} \end{pmatrix}$$

The propagation of $\boldsymbol{y}$ along the coast arc in the interval $(\tau_{\text{MECO}}, \tau_{\text{OMS}})$ is computed by using $\boldsymbol{y}^+_{\text{MECO}}$ as the starting condition. In particular, we will denote such a propagated value of $\boldsymbol{y}$ at τ_{OMS} by $\boldsymbol{y}^-_{\text{OMS}}$. The state and costate along the last powered trajectory in $(\tau_{\text{OMS}}, \tau_f)$ are propagated from $\boldsymbol{y}^+_{\text{OMS}}$. The continuity of the state and costate at τ_{MECO} and τ_{OMS} requires the following two conditions to be met:

$$\boldsymbol{y}^-_{\text{MECO}} - \boldsymbol{y}^+_{\text{MECO}} = 0 \tag{21}$$

$$\boldsymbol{y}^-_{\text{OMS}} - \boldsymbol{y}^+_{\text{OMS}} = 0 \tag{22}$$

The preceding multiple-shooting formulation increases the numbers of unknowns by 24 (the number of scalars included in $\boldsymbol{y}^+_{\text{MECO}}$ and $\boldsymbol{y}^+_{\text{OMS}}$). The continuity condition equations (21) and (22) provide the same number of additional equations. Thus, the dimension of the zero-finding problem is now $8 + 24 = 32$. Note that the solutions for the state and costate in Sec. II.B make the problem completely analytical, from function evaluations to Jacobian computation. The evaluation of the Jacobian requires some care because of the multiple segments of the trajectory. The Appendix provides several useful equations for the part of the Jacobian involving the thrust integrals in Eqs. (15) and (16). The modest dimension of the problem does not constitute a heavy computational requirement that cannot be met more than adequately by a desktop computer (see Sec. VI for some data on CPU time).

In addition to the benefit of enhanced robustness of the algorithm, another advantage of this multiple-shooting formulation of practical significance is the simplicity of the switching condition in Eq. (13) under this setting (see Eq. (28), for example). This feature further contributes to improve the convergence on this condition. And the complexity of the gradient of the switching condition is also reduced notably, particularly so in the case of multiple coast arcs, in which the switching condition will be more complicated [8].

III. Equality Constraints

The unknowns in the problem defined in Sec. II.D are

$$\boldsymbol{z} = (\boldsymbol{\lambda}_0, \boldsymbol{\lambda}^+_{\text{MECO}}, \boldsymbol{x}^+_{\text{MECO}}, \tau_{\text{OMS}}, \boldsymbol{\lambda}^+_{\text{OMS}}, \boldsymbol{x}^+_{\text{OMS}}, \tau_f) \in R^{32} \tag{23}$$

In this section, we list all the 32 equality constraints that $\boldsymbol{z}$ must satisfy to meet the necessary condition of optimal solution and the continuity conditions. The continuity constraints in Eqs. (21) and (22) take the explicit forms of

$$\boldsymbol{s}_1(\boldsymbol{z}) = \Phi(\tau_{\text{MECO}} - \tau_0)\boldsymbol{\lambda}_0 - \boldsymbol{\lambda}^+_{\text{MECO}} = 0 \tag{24}$$

$$\boldsymbol{s}_2(\boldsymbol{z}) = \Phi(\tau_{\text{MECO}} - \tau_0)\boldsymbol{x}_0 + \Gamma(\tau_{\text{MECO}})\boldsymbol{I}^0(\tau_{\text{MECO}}, \tau_0) - \boldsymbol{x}^+_{\text{MECO}} = 0 \tag{25}$$

$$\boldsymbol{s}_3(\boldsymbol{z}) = \Phi(\tau_{\text{OMS}} - \tau_{\text{MECO}})\boldsymbol{\lambda}^+_{\text{MECO}} - \boldsymbol{\lambda}^+_{\text{OMS}} = 0 \tag{26}$$

$$\boldsymbol{s}_4(\boldsymbol{z}) = \boldsymbol{x}_{\text{coast}}(\tau_{\text{OMS}} - \tau_{\text{MECO}}, \boldsymbol{x}^+_{\text{MECO}}) - \boldsymbol{x}^+_{\text{OMS}} = 0 \tag{27}$$

where the thrust integral $\boldsymbol{I}^0(\tau_{\text{MECO}}, \tau_0) = (\boldsymbol{I}_c, \boldsymbol{I}_s)^T$ has its components defined as in Eqs. (15) and (16), with $\boldsymbol{\lambda}_0$ used in the computation of the primer vector $\boldsymbol{p}_V(\cdot)$. The state vector $\boldsymbol{x}_{\text{coast}}(\tau_{\text{OMS}} - \tau_{\text{MECO}}, \boldsymbol{x}^+_{\text{MECO}})$ is the state at τ_{OMS} (the end of coast arc), propagated by the solution of the Kepler's initial value problem from τ_{MECO} with the initial condition $\boldsymbol{x}^+_{\text{MECO}}$ (see Sec. II.C). The scalar switching condition in Eq. (13) is conveniently expressed as

$$S_5(\boldsymbol{z}) = \boldsymbol{\lambda}^{+T}_{\text{OMS}}\boldsymbol{x}^+_{\text{OMS}} = 0 \tag{28}$$

Let $\boldsymbol{\lambda}_f$ and $\boldsymbol{x}_f$ be the final costate and state, determined in $[\tau_{\text{OMS}}, \tau_f]$ through Eqs. (14) and (18) with the initial conditions and $\boldsymbol{\lambda}^+_{\text{OMS}}$ and $\boldsymbol{x}^+_{\text{OMS}}$: that is,

$$\boldsymbol{\lambda}_f = \boldsymbol{\lambda}(\tau_f, \boldsymbol{\lambda}^+_{\text{OMS}}) = \Phi(\tau_f - \tau_{\text{OMS}})\boldsymbol{\lambda}^+_{\text{OMS}} \tag{29}$$

$$\boldsymbol{x}_f = \boldsymbol{x}(\tau_f, \boldsymbol{\lambda}^+_{\text{OMS}}, \boldsymbol{x}^+_{\text{OMS}}) = \Phi(\tau_f - \tau_{\text{OMS}})\boldsymbol{x}^+_{\text{OMS}} + \Gamma(\tau_f)\boldsymbol{I}^{\text{oms}^+}(\tau_f, \tau_{\text{OMS}}) \tag{30}$$

where $\boldsymbol{I}^{\text{oms}^+}(\tau_f, \tau_{\text{OMS}})$ is the thrust integral defined in Eq. (17) by $\boldsymbol{p}_V(\cdot)$ computed in the interval $[\tau_{\text{OMS}}, \tau_f]$ with $\boldsymbol{\lambda}^+_{\text{OMS}}$ as the initial condition.

The k orbital-insertion conditions plus the 6-k equations derivable from the transversality conditions (cf. [9,17,18]) constitute another 6 constraints in the form of

$$\boldsymbol{s}_6(\boldsymbol{z}) = \boldsymbol{s}_6(\boldsymbol{x}_f, \boldsymbol{\lambda}_f) = 0 \tag{31}$$

The specifics of constraints in Eq. (31) depend on the particular set of orbital-insertion conditions. References [17,18] provide some examples in this regard. The last constraint is that the transversality condition on the Hamiltonian $H(\tau_f) = 0$ for the final time τ_f is free. This condition can be simplified by taking into consideration the transversality condition on $p_m(\tau_f)$. Because $m(\tau_f)$ is free, we should have the transversality condition [14]:

$$p_m(\tau_f) = 0$$

Use of this condition and the optimality condition of $\mathbf{1}_T = \boldsymbol{p}_V/\|\boldsymbol{p}_V\|$ in $H(\tau_f) = 0$ based on Eq. (10) leads to the last constraint:

$$S_7(\boldsymbol{z}) = -\omega^2\boldsymbol{\lambda}^T_f\boldsymbol{x}_f + A_T(\tau_f)\|\boldsymbol{p}_V(\tau_f)\| - \frac{T}{c} = 0 \tag{32}$$

where $\boldsymbol{p}_V(\tau_f)$ is the primer vector at τ_f, propagated by Eq. (14) from τ_{OMS} with the initial condition of $\boldsymbol{\lambda}^+_{\text{OMS}}$.

IV. Analysis of the Condition $H(\tau_f) = 0$

The transversality condition $H(\tau_f) = 0$ plays an important role in the problem treated in this paper [i.e., constraint (32)]. Changes in system dynamics due to staging at τ_{MECO} and different numerical scales in $H(\tau_f) = 0$ call for correct understanding of what the condition $H(\tau_f) = 0$ entails and how it can be handled in algorithm implementation. In this section, we provide some detailed analyses related to this condition.

A. $H(\tau_f) = 0$ Does Not Always Mean $H(\tau) = 0$ for All $\tau < \tau_f$

The analysis in Sec. IV is, unless stated otherwise, with regard to the system in Eqs. (1–3) with the performance index in Eq. (9). Using a central-gravity model $\boldsymbol{g}(\boldsymbol{r})$ and the nondimensional formulation, the Hamiltonian of the problem is

$$H = \boldsymbol{p}_r^T \boldsymbol{V} + \boldsymbol{p}_V^T \boldsymbol{g}(\boldsymbol{r})/g_0 + T\left(\frac{\boldsymbol{p}_V^T \mathbf{1}_T}{m g_0} - p_m \frac{1}{c} - \frac{1}{c}\right) := H_0 + TS \tag{33}$$

Because the final mass $m(\tau_f)$ is free, we have $p_m(\tau_f) = 0$. In addition, the optimal thrust direction is given by $\mathbf{1}_T^* = \boldsymbol{p}_V / \|\boldsymbol{p}_V\|$. Hence, the condition $H(\tau_f) = 0$ reduces to

$$H(\tau_f) = \boldsymbol{p}_{r_f}^T \boldsymbol{V}_f + \boldsymbol{p}_{V_f}^T \boldsymbol{g}(\boldsymbol{r}_f)/g_0 + A_T(\tau_f)\|\boldsymbol{p}_{V_f}\| - \frac{T(\tau_f)}{c} = 0 \tag{34}$$

A common misconception is that the transversality condition $H(\tau_f) = 0$ always leads to $H(\tau) = 0$ for all $\tau \in [\tau_0, \tau_f]$ [In this context, the notation $H(\tau)$ is understood to mean $H(\boldsymbol{x}^*(\tau), \boldsymbol{u}^*(\tau), \boldsymbol{p}^*(\tau), \tau)$, where $\{\boldsymbol{x}^*, \boldsymbol{u}^*, \boldsymbol{p}^*\}$ represents the optimal state, control, and costate of the problem.] Although this conclusion is true for *single-phase* free-final-time problems in which the Hamiltonian H is not an explicit function of the independent variable τ, it is *false* for the current burn-coast-burn problem under discussion if there is staging. Recall that the staging between the first stage and second stage occurs at τ_{MECO}. With staging, the system dynamics are different before and after τ_{MECO} because the thrust level and mass rate (i.e., T and c) are usually different from stage to stage, not to mention the mass discontinuity due to the jettison of the first stage. This change of system dynamics can be viewed as being triggered by the condition

$$\xi(\tau) = \tau - \tau_{\text{MECO}} = 0 \tag{35}$$

By following the discussion on optimal control problems with different dynamics in different phases in [21], it can be easily deduced that the Hamiltonian needs to satisfy the jump condition

$$H(\tau_{\text{MECO}}^+) = H(\tau_{\text{MECO}}^-) + \gamma \left.\frac{\partial \xi(\tau)}{\partial \tau}\right|_{\tau=\tau_{\text{MECO}}} = H(\tau_{\text{MECO}}^-) + \gamma \tag{36}$$

where γ is a constant multiplier, and $H(\tau_{\text{MECO}}^-)$ and $H(\tau_{\text{MECO}}^+)$ are the left and right limits (before and after staging) of H at τ_{MECO}, respectively. In fact, it can be readily seen that, because the state and costate are all continuous at τ_{MECO}, and $S(\tau_{\text{MECO}}^-) \neq 0$ when τ_{MECO} is prescribed, the change of system dynamics should certainly cause a discontinuity in the Hamiltonian at τ_{MECO}. Therefore, the transversality condition $H(\tau_f) = 0$ and piecewise constancy of H ensures only that $H(\tau) = 0$ for $\tau \in (\tau_{\text{MECO}}, \tau_f]$. But the jump condition in Eq. (36) suggests that $H(\tau) = -\gamma \neq 0$ for $\tau \in [\tau_0, \tau_{\text{MECO}})$ in general.

An analogous discussion and conclusion can be obtained even for the problem in which multiple burns occur within the same stage (no staging takes place), the burns are separated by coast arcs, and the burn and coast times are prescribed (except for the last burn arc). On the other hand, the condition $H(\tau) = 0$ does hold in the entire interval $[\tau_0, \tau_f]$ in the problem of optimal free-final-time multiburn trajectory, in which the burn and coast times are determined completely by the switching function [cf. Eq. (12)].

The condition $H(\tau) = 0$ is often used to reduce the dimension of the unknowns in the problem or to derive more convenient conditions in optimal trajectories, as it is in this paper in arriving at Eq. (13). One should have a clear and correct understanding of the applicability of the condition $H(\tau) = 0$ whether it is used to design an algorithm or to analyze the problem for multiburn optimal ascent flight.

B. It Is All About Scaling

The condition $H(\tau_f) = 0$ in Eq. (34) [or, similarly, in Eq. (32)] turns out to be a very numerically difficult constraint. This difficulty arises from the fact that, unlike other constraints in Sec. III, Eq. (34) can have a great mismatch in numerical scaling. Specifically, the term $T(\tau_f)/c$ is about 5 orders of magnitude larger than the rest of the terms in Eq. (34) when the state and costate vectors are dimensionless and the costate vector $(\boldsymbol{p}_r^T \ \boldsymbol{p}_V^T)^T$ is chosen to have a magnitude on the order of unity, as is usually done in practice. This difficulty, however, can be alleviated by proper scaling of the problem. The governing equations for the costates in H in Eq. (33) are

$$\boldsymbol{p}_r' = -\frac{\partial H}{\partial \boldsymbol{r}} = -\frac{\partial \boldsymbol{g}^T(\boldsymbol{r})}{g_0 \partial \boldsymbol{r}} \boldsymbol{p}_V \tag{37}$$

$$\boldsymbol{p}_V' = -\frac{\partial H}{\partial \boldsymbol{V}} = -\boldsymbol{p}_r \tag{38}$$

$$p_m' = -\frac{\partial H}{\partial m} = \frac{T\|\boldsymbol{p}_V(\tau)\|}{m^2(\tau) g_0} \tag{39}$$

where the optimality condition $\mathbf{1}_T^* = \boldsymbol{p}_V / \|\boldsymbol{p}_V\|$ has been used in Eq. (39). Clearly, when the vector $(\boldsymbol{p}_r^T \ \boldsymbol{p}_V^T \ p_m)^T$ is scaled by any positive constant, the solutions to the preceding costate equations remain unchanged. If the performance index (9) is also scaled by the same constant, the switching function S in Eq. (33) will stay the same, and hence the optimal solution to the problem will be the same. Thus, if we choose to scale the performance index and $(\boldsymbol{p}_r^T \ \boldsymbol{p}_V^T \ p_m)^T$ by the value of c/T of the second stage and, with some abuse of notation (again), still use $\boldsymbol{p}_V$ and $\boldsymbol{p}_V$ to denote the corresponding vectors after the scaling, transversality condition (34) now becomes

$$H(\tau_f) = \boldsymbol{p}_{r_f}^T \boldsymbol{V}_f + \boldsymbol{p}_{V_f}^T \boldsymbol{g}(\boldsymbol{r}_f)/g_0 + A_T(\tau_f)\|\boldsymbol{p}_{V_f}\| - 1 = 0 \tag{40}$$

This version of the condition $H(\tau_f) = 0$ now admits costate vector $(\boldsymbol{p}_r^T(\tau_f) \ \boldsymbol{p}_V^T(\tau_f))^T$ of a magnitude comparable with those of dimensionless $\boldsymbol{V}_f$ and $\boldsymbol{r}_f$ (on the order of unity).

We shall take the scaling analysis further. In fact, the preceding discussion also shows that the transversality condition $H(\tau_f) = 0$ is equivalent to the following condition for any constant $\kappa_0 > 0$:

$$\boldsymbol{p}_{r_f}^T \boldsymbol{V}_f + \boldsymbol{p}_{V_f}^T \boldsymbol{g}(\boldsymbol{r}_f)/g_0 + A_T(\tau_f)\|\boldsymbol{p}_{V_f}\| - \kappa_0 = 0 \tag{41}$$

Suppose for the moment that the burn-coast-burn problem formulated in Secs. II and III is solved without explicitly using the condition $H(\tau_f) = 0$. Rather, constraint (32) or (34) is replaced by the following condition:

$$\boldsymbol{p}_{r_f}^T \mathbf{V}_f + \boldsymbol{p}_{V_f}^T \boldsymbol{g}(\boldsymbol{r}_f)/g_0 + A_T(\tau_f)\|\boldsymbol{p}_{V_f}\| := H_0(\tau_f) + A_T(\tau_f)\|\boldsymbol{p}_{V_f}\| > 0 \tag{42}$$

Once the problem is solved, let $\kappa_0 = H_0(\tau_f) + A_T(\tau_f)\|\boldsymbol{p}_{V_f}\| > 0$. Then the state and costate solutions so obtained and the positive constant κ_0 satisfy condition (41). In other words, the costate vector $(\boldsymbol{p}_r^T \ \boldsymbol{p}_V^T \ p_m)^T$ and the performance index can be scaled by a positive constant,

$$\kappa_1 = \frac{T(\tau_f)}{\kappa_0 c}$$

so that the scaled variables will precisely meet the condition $H(\tau_f) = 0$ as in the original form in Eq. (34). This way, *all* the necessary conditions of optimality for the problem are now met. Let us formalize this finding:

Property 1: In a free-final-time, minimum propellant consumption, exoatmospheric rocket flight problem, the transversality condition $H(\tau_f) = 0$ is equivalent to the condition in Eq. (42), reproduced next for the convenience of reference:

$$\boldsymbol{p}_{r_f}^T \boldsymbol{V}_f + \boldsymbol{p}_{V_f}^T \boldsymbol{g}(\boldsymbol{r}_f)/g_0 + A_T(\tau_f)\|\boldsymbol{p}_{V_f}\| > 0$$

This property may be of limited practical usefulness by itself. However, we shall show next that under two very reasonable assumptions, condition (42) will be met automatically by the optimal solution without explicit enforcement. Consequently, the condition $H(\tau_f) = 0$ will be satisfied automatically. The two assumptions that we will use to establish our result are as follows:

Assumption 1: The gravity field is a Newtonian inverse-square force field.

Assumption 2: The orbital-insertion conditions in Eq. (8) are such that they satisfy the following condition in the absence of thrust ($T = 0$):

$$\frac{\mathrm{d}\boldsymbol{\phi}(\boldsymbol{r}_f, \boldsymbol{V}_f)}{\mathrm{d}\tau} = \boldsymbol{\phi}'(\tau_f) = 0 \tag{43}$$

Assumption 1 means that the unpowered motion is a Keplerian orbit. Assumption 2 is satisfied when the constraints in $\boldsymbol{\phi}(\boldsymbol{r}_f, \boldsymbol{V}_f)$ are expressed in terms of any of the Keplerian orbital elements such as $a - a_{\text{ref}} = 0$ or $e - e_{\text{ref}} = 0$, where a and e are the semimajor axis and eccentricity, respectively, and a_{ref} and e_{ref} are the specified values for them. In fact, for such a constraint $\phi_i'(\tau) \equiv 0$, $1 \le i \le k$ for $\tau \ge \tau_f$ because of the constancy of the orbital elements. Other cases in which Assumption 2 is met include constraints on the radius and the magnitude of velocity for insertion into a circular orbit, a noncircular (elliptic, parabolic, or hyperbolic) orbit at the periapsis, or an elliptic orbit at the apoapsis. In the case of noncircular orbits, such a constraint meets the condition $\phi_i'(\tau_f) = 0$ only at the orbital-insertion point τ_f. But this is all we need. In other words, most of the typical orbital-insertion conditions can be formed to satisfy Assumption 2.

With this preparation, we are ready to formally make the following claim:

Property 2: Under Assumptions 1 and 2, the condition

$$H_0(\tau_f) = \boldsymbol{p}_{r_f}^T \boldsymbol{V}_f + \boldsymbol{p}_{V_f}^T \boldsymbol{g}(\boldsymbol{r}_f)/g_0 = 0 \tag{44}$$

is always automatically satisfied by the solution to an exoatmospheric optimal ascent problem.

Let us justify the claim. The transversality conditions on the costate are [14]

$$\begin{pmatrix} \boldsymbol{p}_{r_f} \\ \boldsymbol{p}_{V_f} \end{pmatrix} = \begin{pmatrix} \partial \boldsymbol{\phi}^T(\boldsymbol{r}_f, \boldsymbol{V}_f)/\partial \boldsymbol{r}_f \\ \partial \boldsymbol{\phi}^T(\boldsymbol{r}_f, \boldsymbol{V}_f)/\partial \boldsymbol{V}_f \end{pmatrix} \boldsymbol{\nu} \tag{45}$$

where $\boldsymbol{\nu} \in R^k$ is a constant multiplier vector. Using the expressions of $\boldsymbol{p}_{r_f}$ and $\boldsymbol{p}_{V_f}$ from Eq. (45) in $H_0(\tau_f)$, we have

$$H_0(\tau_f) = \boldsymbol{\nu}^T \left[\frac{\partial \boldsymbol{\phi}(\boldsymbol{r}_f, \boldsymbol{V}_f)}{\partial \boldsymbol{r}_f} \boldsymbol{V}_f + \frac{\partial \boldsymbol{\phi}(\boldsymbol{r}_f, \boldsymbol{V}_f)}{\partial \boldsymbol{V}_f} \boldsymbol{g}(\boldsymbol{r}_f) \Big/ g_0 \right] \tag{46}$$

Note that $\boldsymbol{r}_f' = \boldsymbol{V}_f$ and $\boldsymbol{V}_f' = \boldsymbol{g}(\boldsymbol{r}_f)/g_0$ when $T = 0$. So in the absence of thrust, the sum in the preceding equation is equivalent to

$$H_0(\tau_f) = \boldsymbol{\nu}^T \left[\frac{\partial \boldsymbol{\phi}(\boldsymbol{r}_f, \boldsymbol{V}_f)}{\partial \boldsymbol{r}_f} \boldsymbol{r}_f' + \frac{\partial \boldsymbol{\phi}(\boldsymbol{r}_f, \boldsymbol{V}_f)}{\partial \boldsymbol{V}_f} \boldsymbol{V}_f' \right] = \boldsymbol{\nu}^T \boldsymbol{\phi}'(\tau_f) = 0 \tag{47}$$

where Assumption 2 has been used in arriving at this condition. This conclusion is first arrived at in [9] based on an analysis of orthogonality of the final costate vector with respect to the manifold of the admissible variations of the final state vector. Because $H(\tau_f) = H_0(\tau_f) + T(\tau_f)S(\tau_f)$ and $H(\tau_f) = 0$ is a transversality condition for the optimal solution, an immediate corollary of $H_0(\tau_f) = 0$ is that under Assumptions 1 and 2, the switching function satisfies $S(\tau_f) = 0$ along the optimal solution. Note that $S(\tau_f) = 0$ is not always true because τ_f is not an interior switching point.

Because $A_T(\tau_f)\|\boldsymbol{p}_V(\tau_f)\| > 0$, condition (42) is always met if $H_0(\tau_f) = 0$. Combining Property 1 and Property 2, we see that the enforcement of the transversality condition $H(\tau_f) = 0$ is not necessary in finding the solution to the problem of present interest to us and hence the conclusion:

Property 3: In a free-final-time, minimum propellant consumption, exoatmospheric ascent problem in which Assumptions 1 and 2 are satisfied, the transversality condition $H(\tau_f) = 0$ need not be enforced in the solution process.

Based on the preceding conclusion, one of the to-be-determined unknowns in Eq. (23) for the burn-coast-burn problem may be eliminated in correspondence with the removal of the condition $H(\tau_f) = 0$. Instead of doing so, which has no clear and convenient choice, we choose to keep the same unknowns as in Eq. (23). But we pick a simpler and easier replacement to the condition $H(\tau_f) = 0$. Numerous such choices exist. For instance, one could be

$$s_7 = \boldsymbol{p}_V^T(\tau_f)\boldsymbol{p}_V(\tau_f) - c_7 = 0 \tag{48}$$

where $c_7 > 0$ is a constant. The only function of this last constraint is to maintain the same number of equations as the number of unknowns in Eq. (23) and to keep the Jacobian of the constraints nonsingular. Therefore, in the numerical code, we do not even need to actually evaluate s_7 and attempt to enforce $s_7 = 0$. Rather, we can always set $s_7 \equiv 0$ every time the value of s_7 is required; in the case of Eq. (48), this would be equivalent to choosing c_7 to be exactly equal to $\boldsymbol{p}_V^T(\tau_f)\boldsymbol{p}_V(\tau_f)$ each time s_7 is evaluated. When the linear gravity approximation is used, another alternative is to use the constraint

$$s_7 = \boldsymbol{p}_r^T(\tau_f)\boldsymbol{p}_V(\tau_f) + \omega^2 \boldsymbol{p}_V^T(\tau_f)\boldsymbol{p}_V(\tau_f) - 1 = 0 \tag{49}$$

It can be easily shown that the magnitude of the vector $\boldsymbol{\lambda}(\tau) = (\boldsymbol{p}_r^T \omega \boldsymbol{p}_V^T)^T$ is constant under the linear gravity model. Therefore, if the initial value of $\boldsymbol{\lambda}(\tau_0)$ is scaled to have unit length, the constraint in Eq. (49) is trivially met. Such a normalizing constraint is found to be beneficial to convergence when the exoatmospheric algorithm interacts with the endoatmospheric algorithm in a certain way, as described in [10].

In the end, we still have the same number of unknowns in Eq. (23) as the number of constraints $\boldsymbol{s} = (s_1, s_2, s_3, s_4, s_5, s_6, s_7)$, where s_7 is a trivial constraint and the rest are defined in the preceding section.

Finally, as general interest, it is worthwhile to point out that a similar claim can be made for the minimum-time optimal ascent problem for insertion into a Keplerian orbit. In such a problem, the transversality condition on the Hamiltonian is [14]

$$H(\tau_f) = \boldsymbol{p}_{r_f}^T \boldsymbol{V}_f + \boldsymbol{p}_{V_f}^T \boldsymbol{g}(\boldsymbol{r}_f)/g_0 + T(\tau_f)\frac{\boldsymbol{p}_V^T(\tau_f)\boldsymbol{1}_T(\tau_f)}{m(\tau_f)g_0} = 1$$

Suppose that the problem is solved without explicitly enforcing the preceding condition. Property 2 still holds, which, together with $\boldsymbol{1}_T(\tau_f) = \boldsymbol{p}_V(\tau_f)/\|\boldsymbol{p}_V(\tau_f)\|$, leads to

$$H(\tau_f) = T(\tau_f)\frac{\|\boldsymbol{p}_V(\tau_f)\|}{m(\tau_f)g_0} > 0 \tag{50}$$

We now make note of two observations of invariance pertinent to the problem:

1) The costate vector $(\boldsymbol{p}_r^T \ \boldsymbol{p}_V^T)^T$ can be scaled by any constant and the costate equations (37) and (38) are still satisfied;

2) When the costate vector $(\boldsymbol{p}_r^T \ \boldsymbol{p}_V^T)^T$ is scaled by any *positive* constant, the resultant optimal control from the optimality condition and the state trajectory will remain the same.

Hence, if we scale the costate by a positive constant

$$\kappa_2 = \frac{m(\tau_f)g_0}{T(\tau_f)\|\boldsymbol{p}_{V_f}\|} > 0$$

the optimal solution will remain unchanged, and we will now have $H(\tau_f) = 1$ without explicitly enforcing it. Indeed, the maximum principle by Pontryagin et al. [21] only requires $H(\tau_f) > 0$ for the minimum-time problem, which is already met by Eq. (50).

V. Numerical Method

The optimal ascent problem in the preceding section eventually boils down to a multivariate zero-finding problem in which a system of nonlinear algebraic equations is to be solved:

$$\boldsymbol{s}(\boldsymbol{z}) = 0, \qquad \boldsymbol{z} \in R^{32} \tag{51}$$

where $\boldsymbol{s}(\cdot) = (\boldsymbol{s}_1, \boldsymbol{s}_2, \boldsymbol{s}_3, \boldsymbol{s}_4, s_5, \boldsymbol{s}_6, s_7)$: $R^{32} \to R^{32}$ is the smooth vector function defined in Sec. III (and s_7 is defined in Sec. IV). The classical Newton–Raphson method is a common algorithm used for such a purpose. Although simple and effective in many cases, the Newton–Raphson method can suffer from convergence problems when the initial guess is far from the solution and when the Jacobian of system (51) is singular or nearly singular. These problems are handled much better by the renowned Powell's dogleg trust-region method [11]. This method solves the preceding nonlinear equations by minimizing the scalar function F:

$$F(\boldsymbol{z}) = \boldsymbol{s}^T(\boldsymbol{z})\boldsymbol{s}(\boldsymbol{z}) \tag{52}$$

Obviously, the solution to Eq. (51) is the solution to the minimum F. A solution of local minimum for F can exist that is not the solution of Eq. (51) if $F_{\min} \neq 0$. But often times, this is a case in which the solution to Eq. (51) does not exist or the initial guess is very poor. In such a case, one would probably be receptive to taking a solution that minimizes F.

Powell's dogleg method is, in essence, a combination of the Newton and steepest-descent approach. At each iterate $\boldsymbol{z}_k$, the update is constructed as

$$\delta \boldsymbol{z} = \alpha_1 \left(\frac{\partial \boldsymbol{s}}{\partial \boldsymbol{z}}\right)^{-1} \boldsymbol{s}(\boldsymbol{z}_k) + \beta_1 \frac{\partial F}{\partial \boldsymbol{z}}$$

The coefficients α_1 and β_1 are determined in the algorithm. When $\alpha_1 = -1$ and $\beta_1 = 0$, the preceding update reduces to the standard Newton update. This is exactly what the algorithm does whenever the standard Newton update has a size within the trust region. Therefore, the nice quadratic convergence property of the Newton method is preserved when possible. For details of the algorithm, the reader is referred to [11]. In addition to the well-documented superior performance and robustness, other attractive features of this algorithm include the following:

1) An exact Jacobian of system equation (51) is not required. In fact, the Jacobian can even be singular (in such a case, $\alpha_1 = 0$ in the preceding update), a case in which the Newton method will fail.

2) The algorithm will satisfy one of the two stopping criteria in a finite number of iterations. All of these characteristics are appealing in our applications.

We have encountered a number of cases with relatively challenging orbital-insertion conditions for which the Newton method cannot converge. The code with Powell's method, on the other hand, finds the solution readily.

A singularity problem arises in the case in which the optimal coast time is zero. In such a case, the problem loses one parameter ($\tau_{\text{OMS}} = \tau_{\text{MECO}}$) and the switching condition in Eq. (13), and hence Eq. (28), will not be needed. With Powell's method, a simple modification of the formulation can automatically adjust the problem to such a case, and so the same code can be used for cases with and without a coast arc. Define the parameterization

$$\tau_{\text{OMS}} = \frac{\tau_{\text{coast}_{\max}}}{2} \sin \tilde{z}_{19} + \frac{\tau_{\text{coast}_{\max}} + 2\tau_{\text{MECO}}}{2} \tag{53}$$

where $\tau_{\text{coast}_{\max}}$ is a preselected upper bound of the coast time. Clearly, when $\tilde{z}_{19} = -\pi/2$, the preceding $\tau_{\text{OMS}} = \tau_{\text{MECO}}$, and the coast time ($\tau_{\text{OMS}} - \tau_{\text{MECO}}$) is zero. Now let $\tilde{z}_{19}$ replace τ_{OMS} as a parameter to be found. The constraint in Eq. (28) is modified to be

$$s_5 = (1 + \sin \tilde{z}_{19}) \boldsymbol{\lambda}_{\text{OMS}}^{+T} \boldsymbol{x}_{\text{OMS}}^{+} = 0 \tag{54}$$

When the optimal coast time $= 0$, we have $\sin \tilde{z}_{19} = -1$, and $s_5 = 0$ automatically. The problem reduces to a two-burn problem, and Powell's method has no difficulty finding the solution without the need to make any changes to the same burn-coast-burn code. In contrast, this simple approach will cause difficulties for the Newton method, because when $\sin \tilde{z}_{19} = -1$ (thus, $\cos \tilde{z}_{19} = 0$), the gradient of $\partial s_5/\partial \boldsymbol{z}$ is zero and the Jacobian of the problem, $\partial \boldsymbol{s}/\partial \boldsymbol{z} \in R^{32\times 32}$, is singular. As a result, a separate branch of code is required to handle the case in which the optimal coast is close to or equal to zero.

VI. Verification of Algorithm

A. Test Setup

The launch vehicle model used in the simulations is that of a 2-stage vehicle. The first stage has a vacuum thrust of 2.303×10^6 N and the total launch mass is 129,400 kg. The second stage has a vacuum thrust of 2.9269×10^4 N, I_{sp} of 455 s, and the initial overall weight of 5442 kg (after the jettison of the first stage), 1814 kg of which is the vehicle dry weight plus the payload. The launch site is at the Kennedy Space Center. For computation of the optimal ascent trajectory through the atmosphere, the flight of the first stage is tactically divided into two segments: the endoatmospheric portion and exoatmospheric portion, separated at about 70 km in altitude, and the mass of about 70,000 kg. The exoatmospheric portion of the first stage is considered to be the first burn of the exoatmospheric trajectory in the context of the problem formulation in this paper, and the second burn is the second stage of the launch vehicle. The endoatmospheric solution is obtained by the methodology described in [10,18]. For different orbital-insertion conditions, the endoatmospheric trajectory results in somewhat different initial conditions for a subsequent exoatmospheric trajectory. The analytical multiple-shooting (AMS) algorithm described in this paper is used to determine the optimal burn-coast-burn trajectory thereafter.

To verify the results found by the AMS algorithm, an industry-standard aerospace trajectory optimization software, called Optimal Trajectories by Implicit Simulation [12] (OTIS), is employed to compute the burn-coast-burn trajectory under identical conditions. Further comparison is done with closed-loop simulated trajectories. In the closed-loop simulations, the AMS algorithm serves as the guidance algorithm, generating the optimal exoatmospheric trajectory from the current state to the orbital-insertion point at a guidance cycle of 1 Hz. The actual trajectory is simulated by integrating Eqs. (1–3) with an inverse-square gravity field. The optimal thrust direction and throttle command (full thrust or coast) are determined by the AMS algorithm. The closed-loop simulations are an ultimate check for the validity of the open-loop solution found. If the closed-loop trajectory matches the open-loop trajectory closely, the approximations adopted in obtaining the open-loop solution are well justified.

The target orbit in each of the testing cases has the required orbital elements listed in Table 1. In the case of elliptic orbit, the insertion point is specified at the perigee. Therefore, the values of the semimajor axis and eccentricity in case 4 are such that the orbital-insertion altitude is the same as that in case 1, and case 5 is the same as in case 2 (of course, the insertion velocities are different.)

B. Test Results

The test results for the five cases in Table 1 using AMS and OTIS are listed in Table 2. Recall that the burn time of the first vacuum stage is fixed. Thus, for each case, Table 2 gives just the coast time and burn time of the second vacuum stage, which are optimized. The

Table 1 Target orbits in the testing cases ($R_0 = 6378.135$ km is the radius of the Earth)

Case	a semimajor axis, km	e eccentricity	Inclination, deg
1	$R_0 + 300$	0	51.6
2	$R_0 + 500$	0	51.6
3	$R_0 + 1000$	0	51.6
4	$R_0 + 1042.015$	0.1	51.6
5	$R_0 + 1264.237$	0.1	51.6

Table 2 Comparison of test results

Case	Method	Coast time, s	Second vacuum burn time, s
Case 1	OTIS	76.53	281.07
	AMS	77.79	281.15
	AMS closed-loop	81.29	285.85
Case 2	OTIS	138.28	308.10
	AMS	152.02	307.35
	AMS closed-loop	157.58	311.70
Case 3	OTIS	242.46	368.72
	AMS	217.08	371.24
	AMS closed-loop	230.57	375.12
Case 4	OTIS	76.98	315.16
	AMS	63.73	316.18
	AMS closed-loop	68.58	320.75
Case 5	OTIS	148.17	337.67
	AMS	138.58	338.81
	AMS closed-loop	142.82	343.34

difference in the burn time of the second stage therefore directly translates into the difference in the orbital-insertion mass. Closed-loop simulation under AMS guidance is also performed for every case and the results are shown as well. For case 1, the open-loop AMS and OTIS solutions are essentially the same. OTIS uses a direct approach to the optimal control problem by a collocation method. The AMS, on the other hand, is an indirect approach that solves the optimal control problem based on the necessary conditions. The extent to which the results from these two different methods match this well is certainly quite noteworthy. The closed-loop simulation for case 1 shows quite reasonable closeness to the open-loop solution. The slightly longer burn time of the second stage in the closed-loop trajectory is to be expected because the vehicle dynamics are in full effect in closed-loop simulations. The fact that the closed-loop burn time is consistently about 4 s or more longer than the AMS open-loop burn time in all the cases, as can be seen from Table 2, indicates such an effect.

The performance index on the final mass in the optimal burn-coast-burn problem appears to be relatively insensitive to the coast time. An appreciable change in the coast time only causes a disproportionately small variation in the orbital-insertion mass. The test results for cases 2 and 3 in Table 2 exemplify such insensitivity. The solutions by AMS and OTIS differ noticeably in the coast time, but the differences in the second burn time are much smaller (thus, there are small differences in the final mass). Because direct methods such as OTIS optimize the performance index directly over the optimization variables, we have found that such a "flat optimum" tends to cause OTIS to converge in the same problem to different solutions, most notably in terms of the coast time, depending on the setting of the input. Appropriate scaling of the variables, which we have not performed, may help rectify this problem. On the other hand, the AMS algorithm, an indirect method, does not appear to suffer from this problem, yielding the same solution consistently for the same case regardless of the changes in the initial guess.

Another noteworthy comparison between OTIS and AMS is the execution time. Implemented in FORTRAN, the AMS algorithm takes about 0.03 s or less CPU time on a desktop computer to find the solution from a relatively poor initial guess. OTIS (also in FORTRAN) can take up to 600 s or longer CPU time to find a solution. It is recognized that OTIS is designed to be a general-purpose aerospace trajectory optimization tool, and thus it carries overhead in CPU usage. But the 5-orders-of-magnitude-faster execution speed of the AMS algorithm is still remarkable.

Figure 2 shows the closed-loop ascent trajectories for case 1–case 3 (only the exoatmospheric portion of the complete ascent trajectory). During the coast arc, the vehicle exchanges kinetic energy for potential energy by gaining altitude. The higher the orbital-insertion altitude, the longer the coast arc tends to be, and the more pronounced the effect of the optimal coast. For instance, for case 3, the orbital-insertion mass would be 473 kg less if the optimal trajectory does not include a coast, a 23% reduction in payload delivery capability.

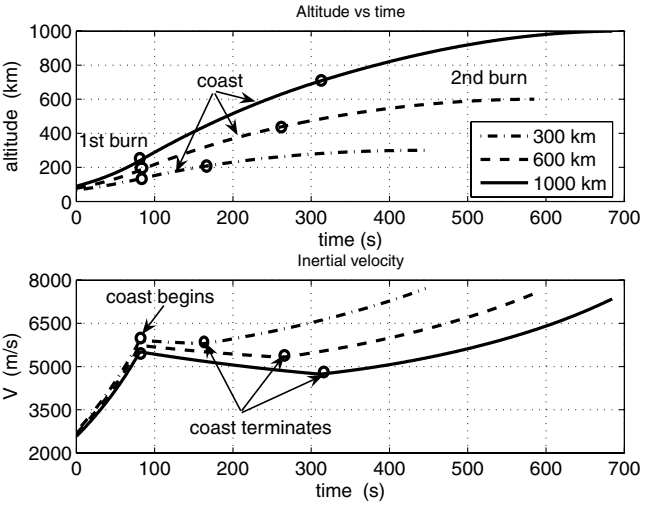

Fig. 2 Altitude and velocity profiles of the closed-loop burn-coast-burn ascent trajectories for insertion into circular orbits.

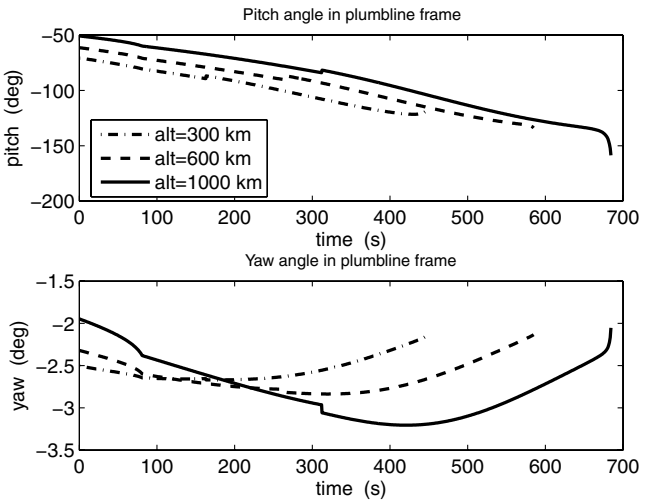

Fig. 3 Pitch and yaw angles along the closed-loop burn-coast-burn ascent trajectories with respect to the launch plumb-line frame (circular orbit insertion).

Figure 3 depicts the pitch- and yaw-angle histories of the vehicle body axes with respect to the launch plumb-line frame along the closed-loop trajectories for case 1–case 3. The launch plumb-line frame is an Earth-centered inertial frame. Its x axis is parallel to the local vertical direction at the launch site, the z axis is in the direction of the launch azimuth at the launch site, and the y axis completes a right-hand system (in the out-of-plane direction.) The body frame is initially aligned with the plumb-line frame. The rotation sequence of 2-3-1 is used in defining the pitch and yaw angles. From Fig. 3, it is seen that the yaw angle is generally very small. This is due to the fact the launch azimuth is oriented in the direction defined by the target orbit inclination to minimize the yaw maneuvers, a common practice in launch vehicle operations.

VII. Conclusions

This paper presents a robust and fast algorithm for finding optimal exoatmospheric burn-coast-burn ascent trajectories. A traditional single-shooting formulation for this problem suffers from convergence problems due to heightened sensitivity in the presence of coast arcs. The analytical multiple-shooting approach taken in this paper provides an alternative with the potential for a much-improved algorithm. An in-depth analysis of the optimal ascent problem reveals properties of the problem that allow one to circumvent the

numerical difficulty caused by a scaling mismatch in one of the transversality conditions. This step is found to be crucial in leading to the enhanced convergence reliability of the algorithm. Employment of Powell's trust-region root-finding method further adds to the ability of the algorithm to handle nearly singular and singular cases (when the optimal coast time reduces to zero) and poor initial guesses. Comparison of the numerical results with those from an existing standard trajectory optimization tool verifies the algorithm. The proposed algorithm appears to offer a promising tool for rapid launch mission planning and fully autonomous closed-loop ascent guidance in missions involving long coast and multiple burns.

Appendix: Jacobians of Thrust Integrals

In the numerical solution of the burn-coast-burn problem in this paper, the Jacobian of the constraint vector in Eq. (51) can be analytically obtained. Although much of it just requires standard (and careful) vector differentiation, the most involved part is perhaps the Jacobians of the thrust integrals in Eqs. (15) and (16). This Appendix provides the key equations that are very useful in analytically computing these Jacobians (see [17] for some similar results). Consider the thrust integrals in an interval $[\tau_1, \tau_2]$:

$$\boldsymbol{I}_c(\tau_2, \tau_1) = \int_{\tau_1}^{\tau_2} \mathbf{1}_{p_V}(\zeta) \cos(\omega\zeta) A_T(\zeta)\, \mathrm{d}\zeta \in R^3 \tag{A1}$$

$$\boldsymbol{I}_s(\tau_2, \tau_1) = \int_{\tau_1}^{\tau_2} \mathbf{1}_{p_V}(\zeta) \sin(\omega\zeta) A_T(\zeta)\, \mathrm{d}\zeta \in R^3 \tag{A2}$$

Let $\boldsymbol{\lambda}_1 = \mathrm{col}(\boldsymbol{p}_V(\tau_1), \ -\boldsymbol{p}_r(\tau_1)/\omega)$ be the initial costate vector in this interval, and let h be a step-size parameter defined as

$$h = \frac{\tau_2 - \tau_1}{N}$$

where $N = 2$ for using Simpson's rule to compute the preceding integrals and $N = 4$ for Milne's rule. Define the following matrices for $i = 0, 1, \ldots, N$ in $R^{3\times 6}$:

$$\Lambda(ih) = [\cos(i\omega h) I_{3\times 3} \ \sin(i\omega h) I_{3\times 3}] \tag{A3}$$

$$K(\tau_1 + ih) = \frac{1}{\|\boldsymbol{p}_V(\tau_1 + ih)\|}[I_{3\times 3} - \mathbf{1}_{p_V}(\tau_1 + ih)\mathbf{1}_{p_V}^T(\tau_1 + ih)]\Lambda(ih) \tag{A4}$$

Through the thrust direction $\mathbf{1}_{p_V}(\tau) = \boldsymbol{p}_V(\tau)/\|\boldsymbol{p}_V(\tau)\|$, both $\boldsymbol{I}_c$ and $\boldsymbol{I}_s$ are functions of $\boldsymbol{\lambda}_1$. When these integrals are evaluated by a numerical quadrature method, it can be shown that the Jacobians of $\boldsymbol{I}_c$ and $\boldsymbol{I}_s$ with respect to $\boldsymbol{\lambda}_1$ are given by

$$\frac{\partial \boldsymbol{I}_c(\tau_2, \tau_1)}{\partial \boldsymbol{\lambda}_1} = \frac{(\tau_2 - \tau_1)}{n_s} \sum_{i=0}^{N} b_i A_T(\tau_1 + ih) \cos(\tau_1 + i\omega h) K(\tau_1 + ih) \tag{A5}$$

$$\frac{\partial \boldsymbol{I}_s(\tau_2, \tau_1)}{\partial \boldsymbol{\lambda}_1} = \frac{(\tau_2 - \tau_1)}{n_s} \sum_{i=0}^{N} b_i A_T(\tau_1 + ih) \sin(\tau_1 + i\omega h) K(\tau_1 + ih) \tag{A6}$$

where, for Milne's rule, we have

$$N = 4, \quad n_s = 90, \quad b_0 = 7, \quad b_1 = 32, \quad b_2 = 12$$
$$b_3 = 32, \quad b_4 = 7$$

and for Simpson's rule,

$$N = 2, \quad n_s = 6, \quad b_0 = 1, \quad b_1 = 4, \quad b_2 = 1$$

Acknowledgments

The authors at Iowa State University acknowledge the support to this research by the U.S. Air Force Research Laboratory, Space Vehicles Directorate, Kirtland Air Force Base, New Mexico, through contract FA9453-05-0268 P00002. The gracious help offered by Steve Paris on the use of Optimal Trajectories by Implicit Simulation (OTIS) software is appreciated.

References

[1] Smith, I. E., "General Formulation of the Iterative Guidance Mode," NASA TM X-53414, Mar. 1966.

[2] McHenry, R. L., Brand, T. J., Long, A. D., Cockrell, B. F., and Thibodeau, J. R., III, "Space Shuttle Ascent Guidance, Navigation, and Control," *Journal of the Astronautical Sciences*, Vol. 27, No. 1, 1979, pp. 1–38.

[3] Brown, K. R., Harrold, E. F., and Johnson, G. W., "Rapid Optimization of Multiple-Burn Rocket Trajectories," NASA CR-1430, Sept. 1969.

[4] Jezewski, D. J.,"Optimal Analytic Multiburn Trajectories," *AIAA Journal*,Vol. 10, No. 5, 1972, pp. 680–685. doi:10.2514/3.50176

[5] Jezewski, D. J.,"N-Burn Optimal Analytic Trajectories" *AIAA Journal*, Vol. 11, No. 10, 1973, pp. 1373–1376. doi:10.2514/3.50595

[6] McAdoo, S. F., Jezewski, D. J., and Dawkins, G. S., "Development of a Method for Optimal Maneuver Analysis of Complex Space Missions," NASA TN D-7882, Apr. 1975.

[7] Gath, P. F., and Calise, A. J., "Optimization of Launch Vehicle Ascent Trajectories with Path Constraints and Coast Arcs," *Journal of Guidance, Control, and Dynamics*, Vol. 24, No. 2, 2001, pp. 296–304.

[8] Dukeman, G., and Calise, A., "Enhancements to an Atmospheric Ascent Guidance Algorithm," AIAA Paper 2003-5638, Aug. 2003.

[9] Dukeman, G., "Closed-Loop Nominal and Abort Atmospheric Ascent Guidance for Rocket-Powered Launch Vehicles," Ph.D. Dissertation, Georgia Inst. of Technology, Atlanta, May 2005.

[10] Lu, P., Zhang, L., and Sun, H., "Ascent Guidance for Responsive Launch: a Fixed-Point Approach," AIAA Paper 2005-6453, Aug. 2005.

[11] Powell, M. J. D., "A Hybrid Method for Nonlinear Equations," *Numerical Methods for Nonlinear Algebraic Equations*, edited by Rabinpwitz, P., Gordon and Breach, New York, 1970, p. 87–114.

[12] Hargraves, C. R., and Paris, S. W., "Direct Trajectory Optimization Using Nonlinear Programming and Collocation," *Journal of Guidance, Control, and Dynamics*, Vol. 10, No. 4, 1987, pp. 338–342. doi:10.2514/3.20223

[13] Jezewski, D. J.,"An Optimal, Analytic Solution to the Linear Gravity, Constant-Thrust Trajectory Problem," *Journal of Spacecraft and Rockets*, Vol. 8, No. 7, 1971, pp. 793–796. doi:10.2514/3.30320

[14] Bryson, A. E., and Ho, Y. C., *Applied Optimal Control*, Hemisphere, Washington, D.C., 1975, pp. 42–87.

[15] Lawden, D. F., *Optimal Trajectories for Space Navigation*, Butterworths, London, 1963, pp. 54–68.

[16] Robbins, H. M., "Optimality of Intermediate-Thrust Arcs of Rocket Trajectories," *AIAA Journal*, Vol. 3, No. 6, 1965, pp. 1094–1098. doi:10.2514/3.3060

[17] Leung, M. S. K., and Calise, A. J., "Hybrid Approach to Near-Optimal Launch Vehicle Guidance," *Journal of Guidance, Control, and Dynamics*, Vol. 17, No. 5, 1994, pp. 881–888. doi:10.2514/3.21285

[18] Lu, P., Sun, H., and Tsai, B., "Closed-Loop Endo-Atmospheric Ascent Guidance," *Journal of Guidance, Control, and Dynamics*, Vol. 26, No. 2, 2003, pp. 283–294.

[19] Danby, J. M. A., *Fundamentals of Celestial Mechanics*, 2nd ed., Willmann-Bell, Richmond, VA, 1988, pp. 162–177.

[20] Goodyear, W., "Completely General Closed-Form Solution for Coordinates and Partial Derivatives of the Two-Body Problem," *Astronomical Journal*, Vol. 70, No. 3, 1965, pp. 189–192. doi:10.1086/109713

[21] Pontryagin, L. S., Boltyanskii, V. G., Gramkreledze, Q. V., and Mishchenko, E. F., *The Mathematical Theory of Optimal Processes*, Intersciences, New York, 1962, pp. 20–21, 311–316.